CHAPTER 7

CHARACTERISATION OF PARAMETERS

The accuracy of the mathematical models depended strongly on the accuracy of the input data. For this reason, the finite element analysis was not sufficient proof of the parameters for the components. Certain components could also not be accurately modelled due to unavailability of material specifications.

The components of the experimental setup therefore needed to be experimentally characterised to check the values obtained from the finite element analysis and to determine the parameters of the components not modelled.

7.1. Mass of components

The most basic parameter to characterise, was the mass of the different vibration model components. These values had to be combined according to the definitions in Section 5 to give the element masses needed for the theoretical simulation.

7.1.1. Mass of components

Each individual component was placed on an electronic scale to determine its mass. The accuracy of the scale was firstly determined with the help of a standard (5 kg) mass, as can be seen in Figure 49.

Figure 49: Validation of the accuracy of the electronic scale

Each of the components was weighed individually and their masses noted, as can be seen in Figure 53.

Figure 50: Measured mass of the top frame

Figure 51: Measured mass of the bottom frame

Figure 52: Measured mass of the plate pack

Figure 53: Measured mass of the vibrating motor

The measured values is summarised in Table 2.

Table 2: Measured mass properties of model

Mass of top frame [kg]	m_T	11.856
Mass of bottom frame [kg]	m_b	2.294
Total mass of plate pack [kg]	m_p	25.838
Mass of electric motor [kg]	m_m	6.274
Total mass of model [kg]	m_{Tot}	46.262

7.1.2. Mass of elements

With the mass of the components known, the equations in Section 5 could be used to determine all the mass elements of the mathematical model.

The most critical value to determine was the effective mass relating to the vibration caused by the vibrating motor.

The model was assembled in the stiff steel-mounted configuration without the bottom compensator, as illustrated in Figure 66.

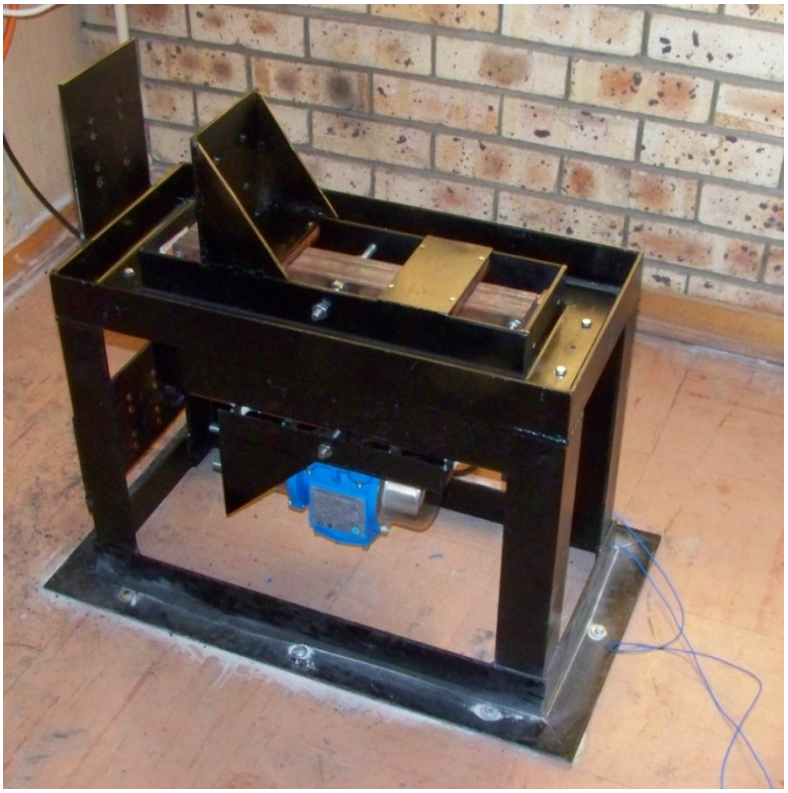

Figure 54: Experimental setup used to determine effective mass

The model was then subjected to a bump test in the direction normal to the plates to determine the natural response of the plate pack. The

resulting frequency response is shown in Figure 55, clearly indicating the natural frequency at about 18.375 Hz (115.454 rad/s).

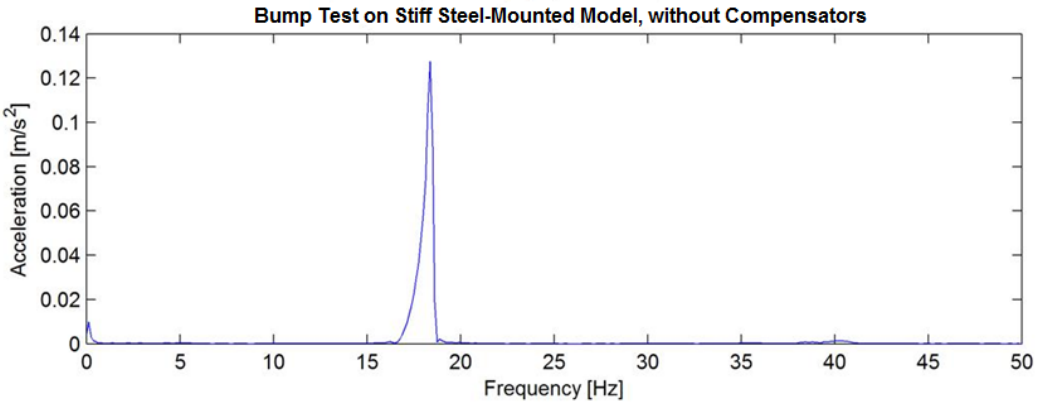

Figure 55: Measured frequency response of bump test on stiff steel-mounted model, without compensators

At a constant forcing frequency of 30 Hz (188.496 rad/s), the resulting acceleration was measures on the bottom frame. The resulting frequency plot for the acceleration is shown in Figure 56, indicating an amplitude of 5.302 $m.s^{-2}$.

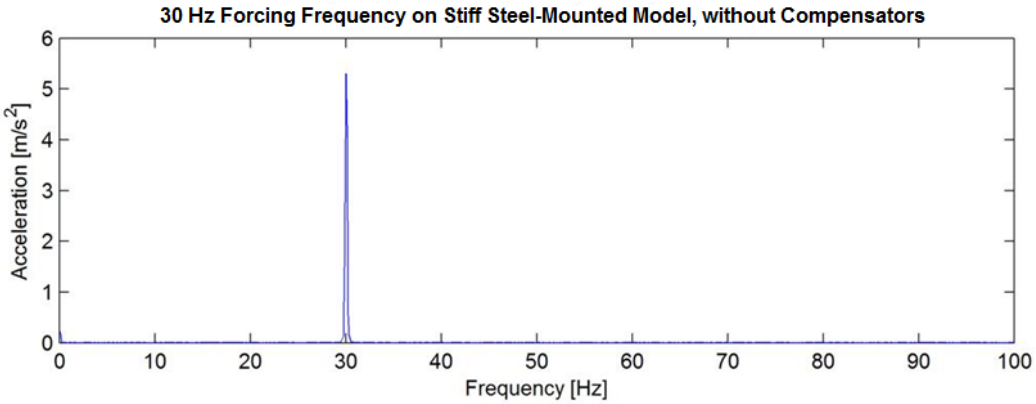

Figure 56: Measured frequency plot for acceleration measurements for a forcing frequency of 30 Hz

From the measured results in the two previous diagrams, using Equation (5.12) and the characterised unbalanced load from Section 7.6, the resulting effective mass of the model can be determined. The calculation of the effective model mass (m_2) from the measured values in the stiff steel-mounted condition is shown in Table 3.

Table 3: Calculation of effective mass of model under stiff steel-mounted condition

Unbalaced load factor [kg/m]	$m_u r$	0.002238244
Natural frequency of model [rad/s]	ω_n	115.454
Forcing frequency [rad/s]	ω	188.496
Measured acceleration amplitude [m.s^{-2}]	$\ddot{X}$	5.302
Effective model mass in bolted condition[kg]	m_2	24.007

With the value of m_2 determined, the other element masses could also be calculated with Equations (5.3) to (5.6), as shown in Table 4.

Table 4: Calculation of other elements' mass

Mass connected to bottom frame [kg]	m_1	22.255
Mass connected to top frame [kg]	m_2	24.007
Plate pack mass contribution to m_1 [kg]	m_r	10.399
Plate pack mass contribution to m_2 [kg]	m_e	15.439
Total mass of model [kg]	m_{Tot}	46.262

7.2. Characterisation of plate-pack

The plate pack was fully characterised by using the same bump test results as was used to determine the effective mass of the stiff steel-mounted model. This is due to the fact that the plate pack was assumed to be the only source of flexibility in the stiff steel-mounted configuration without compensators.

7.2.1. Stiffness

The results of the bump test, illustrated in Figure 55, indicated a natural frequency of 18.375 Hz (115.454 rad/s). If this were considered together with the effective mass of the system in this configuration, the stiffness of the plate pack can be calculated as shown in Table 5.

Table 5: Calculation of stiffness of plate pack

Measured natural frequency [rad/s]	ω_n	115.454
Calculated effective mass [kg]	m_2	24.007
Stiffness of plate pack [N/m]	k_p	319997

With the stiffness of the plate pack determined, the value of k_2 could be determined from Equation (5.15), as shown in Equation (7.1).

$$k_2 = 319997 \text{ N/m} \tag{7.1}$$

The assumed stiffness k_{1R} was also defined in terms of k_p in Equation (5.14), making it possible to determine k_{1R} as shown in Equation (7.2).

$$k_{1R} = 319997000 \text{ N/m} \tag{7.2}$$

7.2.2. Damping coefficient

The damping ratio of the plate pack had to be determined from the measured time spectrum of the bump test used above to determine the stiffness of the plate pack. Figure 57 illustrates the time spectrum response of the bump test that could be used to calculate the damping characteristics of the plate pack.

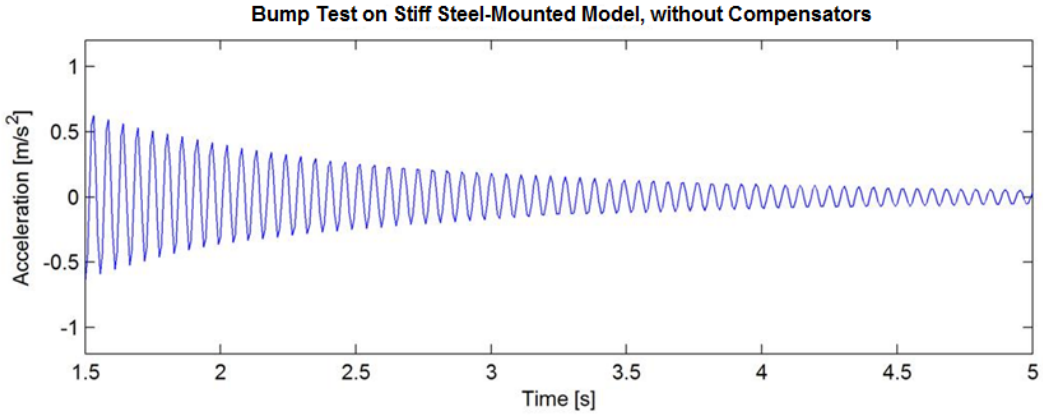

Figure 57: Measured time response of bump test without compensator

The raw data of the measurements were used to obtain the exact peak values of twenty cycles of the response. These values were used to determine the damping characteristics of the plate pack. The full calculation is shown in Appendix E, with the results summarised in Table 6.

Table 6: Characterised damping parameters for the plate pack (Appendix E)

Natural frequency [Hz]	f_n	18.29
Natural frequency [rad/s]	ω_n	114.89
Equivalent mass [kg]	m_2	24.007
Damping factor [Ns/m]	c_p	43.699
Damping ratio	ζ_p	0.008

From the damping ratio of the plate pack (c_p), the value of c_2 could be determined by using Equation (5.29), as shown in equation (7.3).

$$c_2 = 43.699 \text{ N.s/m} \tag{7.3}$$

7.3. Characterisation of mounts

The characteristics of rubber mounts are dependent on the load that is applied to them. It was therefore important to ensure that the mounts were characterised under the same conditions that they were going to be used.

For this reason, the mounts were characterised while they were supporting the whole model (as they would under test conditions). The compensators (top and bottom) were not connected to ensure that they would not influence the experiment. A bump test was conducted in the same direction as the expected vibration (normal to the plates). The experimental setup can be seen in Figure 58.

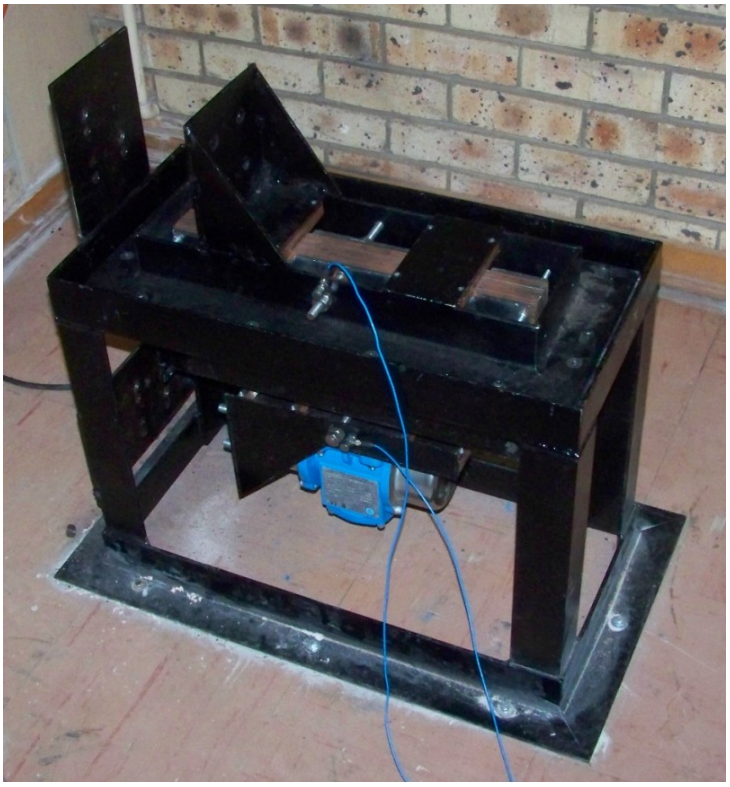

Figure 58: Experimental setup used for the characterisation of mounts

7.3.1. Stiffness

The measured frequency response of the bump test is indicated in Figure 59.

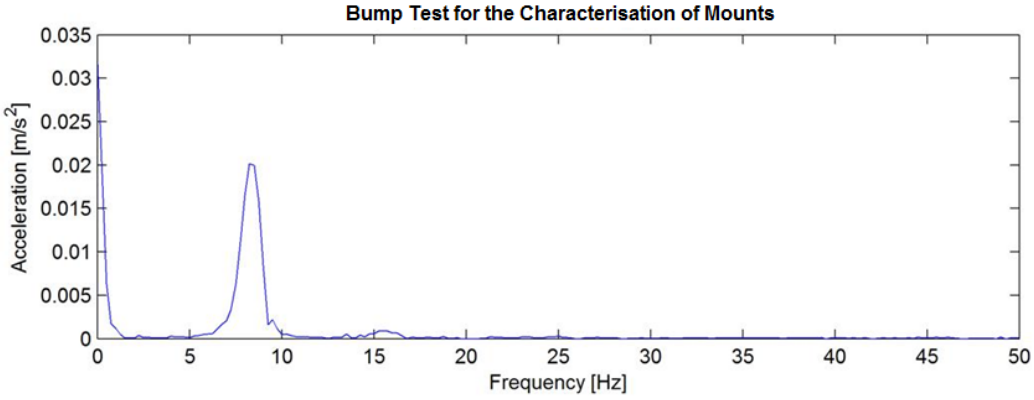

Figure 59: Measured frequency response of bump test for characterisation of mounts

From the results, the natural frequency of the system can clearly be seen at about 8.25 Hz (51.836 rad/s). This value was used, together with the total mass of the model, to determine the stiffness of all the mounts together. This value was converted to the individual stiffness of the mounts. This calculation can be seen in Table 7.

Table 7: Calculation of mount stiffness characteristics

Mass [kg]	m_{Tot}	46.262
Number of mounts	N_m	6
Natural frequency [Hz]	f_n	8.25
Natural frequency [rad/s]	ω_n	51.84
Stiffness of all mounts [N/mm]	k_m	124.306
Stiffness of individual mounts [N/mm]	k_{mi}	20.718

Because the model was free to vibrate in any of the 6 degrees of freedom, the values obtained was evaluated to ensure that the correct mode shape was evaluated.

According to the mount catalogue, these specific mounts should have a lateral stiffness of 20 N/mm. The calculated value compares extremely well with this value and it was seen as a confirmation that the correct mode shape was excited.

7.3.2. Damping coefficient

The measured Time response is shown in Figure 60.

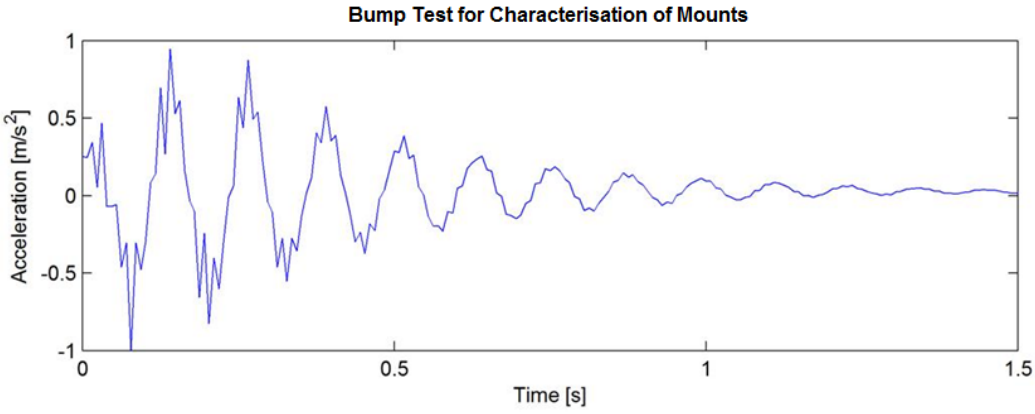

Figure 60: Measured time response for bump test used to characterise mounts

The raw data was used to obtain the maximum and minimum peak values for eight cycles, providing 16 points that were used to determine the damping ratios. The combined values determined were converted into individual damping ratios for each of the mounts. The full calculation is shown in Appendix F with the results summarised in Table 8.

Table 8: Calculation of the damping ratio of mounts (Appendix F)

Natural frequency [Hz]	f_d	8.24
Natural frequency [rad/s]	ω_d	51.77
Mass of model [kg]	m_{Tot}	46.262
Number of mounts	N_m	6
Damping factor of all mounts [Ns/m]	c_m	273.451
Damping factor of individual mount [Ns/m]	c_{mi}	45.575
Damping ratio of mounts	ζ_{mi}	0.057

7.4. Characterisation of pipe compensators

The pipe compensators were regarded as very critical components in the system, as they contribute an amount of damping to the system. The bottom compensator is situated on the anti node-point of the mode of vibration.

Instead of using a bump test to characterise the pipe compensators as in the previous case, the pipe compensators were characterised using a shaker test setup. The test setup consisted of a mass suspended by two pipe compensators mounted in a very stiff frame, as shown in Figure 61.

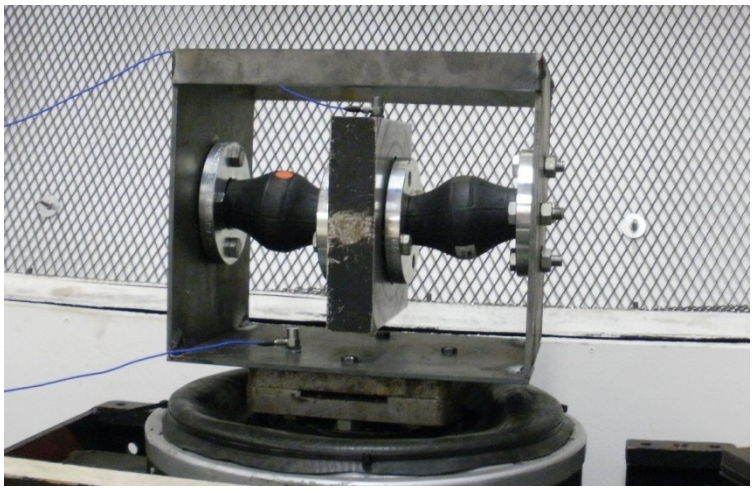

Figure 61: Experimental setup for pipe compensator characterisation

The mass used to characterise the compensators, was 11.404 kg, machined to ensure that it fit securely between the two compensators in a stiff frame, with the holes as accurate as possible to ensure that no rotational mode shapes were excited.

The acceleration of both the mass and the base plate was measured with two acceleration meters and analysed with a two-channel FFT

analyser. The amplitude of the displacements of the vibration measured by the two acceleration meters (X and Y) and the phase angle (ϕ) could be used to determine the stiffness and damping coefficient of the pipe compensators by using Equations (7.1) and (7.2) (Rao, 2004).

$$\frac{X}{Y} = \left[\frac{k^2 + (c\varpi)^2}{\left(k - m\varpi^2\right)^2 + (c\varpi)^2} \right]^{1/2} \tag{7.1}$$

$$\phi = \tan^{-1}\left[\frac{mc\varpi^3}{k\left(k - m\varpi^2\right) + (\varpi c)^2} \right] \tag{7.2}$$

The measured vibration values of the test mass ($\ddot{X}$) mass and the base ($\ddot{Y}$) is shown in Figure 62. From these results the amplitudes of the vibration could be determined for the test mass (X) and for the base (Y), which could be used in Equation (7.1).

From the time spectrum measurements shown in Figure 63, the phase angle between the two vibration wave forms (ϕ). The phase angle between the two waves can be substituted into Equation (7.2).

By simultaneously solving Equations (7.1) and (7.2), the vibration parameters of the pipe compensators could be determined. The results are reported in Table 9.

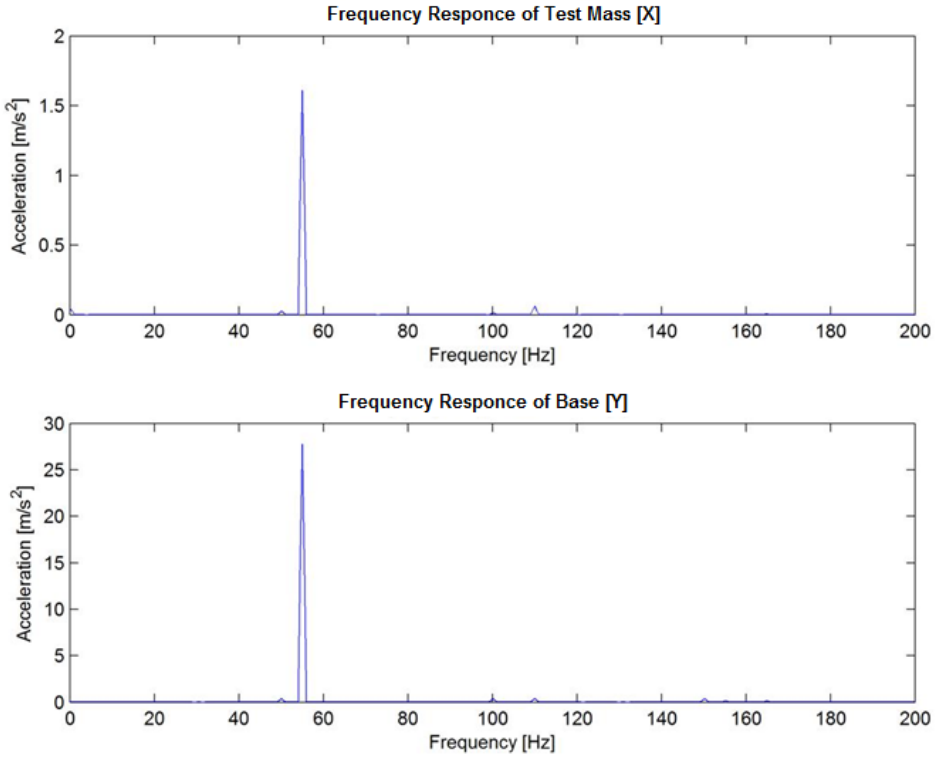

Figure 62: Measured frequency spectra of the shaker test

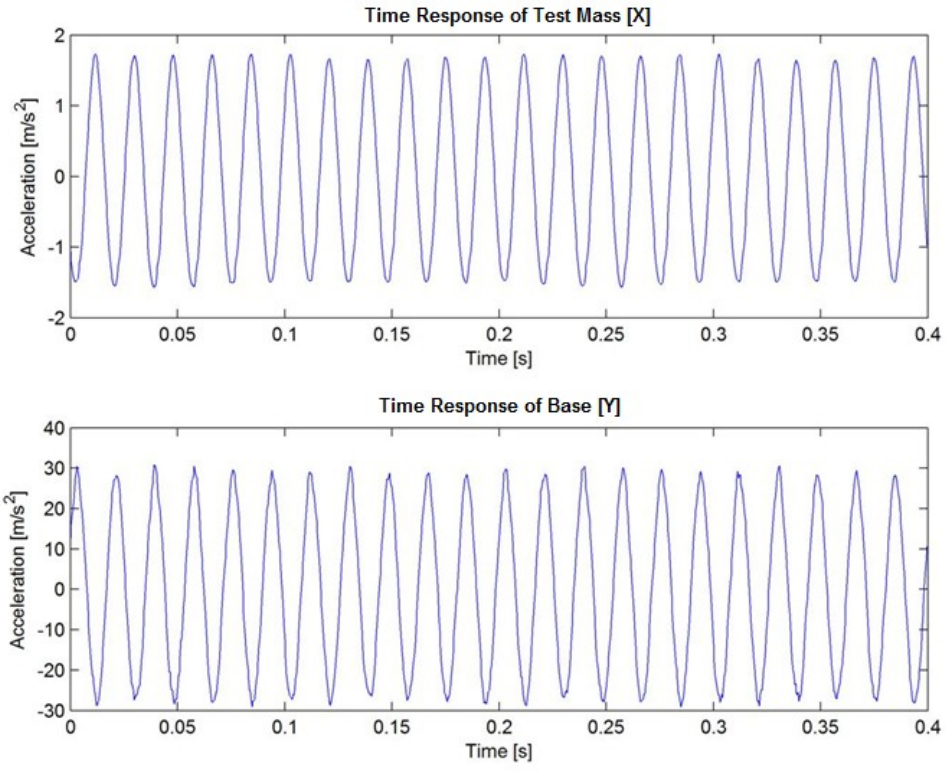

Figure 63: Measured time response of shaker test for the base and the test mass

Table 9: Calculation of vibration parameters of compensators

Mass [kg]	m	11.404
Frequency [Hz]	f	55
Number of compensators	N_c	2
Acceleration amplitude of test mass [m/s^2]	$\ddot{X}$	1.609
Acceleration amplitude of base [m/s^2]	$\ddot{Y}$	27.664
Displacement amplitude of test mass [m]	X	1.347E-05
Displacement amplitude of base [m]	Y	2.317E-04
Phase angle [rad]	φ	2.903
Stiffness of all compensators [N/mm]	k_c	73.058
Stiffness of individual compensator [N/mm]	k_{ci}	36.529
Damping factor of all compensators [Ns/m]	c_c	48.552
Damping factor of individual compensators [Ns/m]	c_{ci}	26.830
Damping ratio of compensators	ζ_c	0.027

With the value of k_{ci} together with the value of k_{mi} (from Table 7), the value of k_{1M} could be determined, using Equation (5.13), as can be shown in Equation (7.4).

$$k_{1M} = 160837 \text{ N/m} \tag{7.4}$$

In the same way the value of k_3 could also be determined by using Equation (5.16), as can be shown in Equation (7.5).

$$k_3 = 36529 \text{ N/m} \tag{7.5}$$

As the value of C_{ci} was also determined, while the values of C_{1M} and C_3 could be calculated by using Equations (5.28) and (5.30) respectively. The values are indicated in Equations (7.6) and (7.7).

$$C_{1M} = 300.280 \text{ N.s/m} \tag{7.6}$$

$$c_3 = 26.830 \text{ N.s/m} \tag{7.7}$$

7.5. Characterisation of whole heat exchanger model

With all the components characterised individually, the heat exchanger as a whole mounted with the mounts and compensators was characterised by doing a bump test.

Figure 64: The rubber mounts and compensators used to isolate the model from the frame

Figure 65: Location of rubber mounts on frame

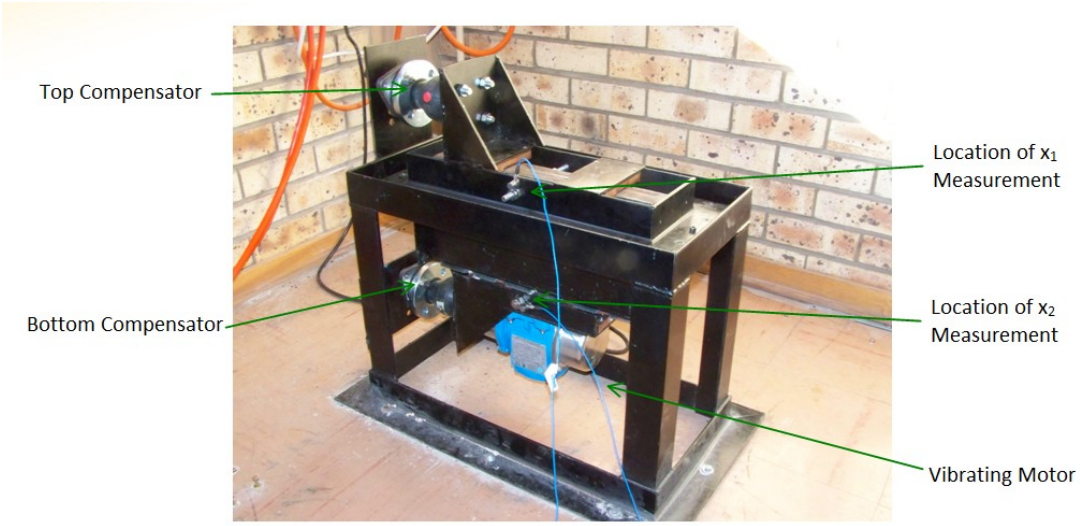

Figure 66: Experimental setup used for the bump test of whole model

With this setup, the system was excited with a rubber hammer on the electric motor connected to the bottom frame. The accelerator that was used, was connected to the bottom frame (x_2 position), with the results illustrated in Figure 67.

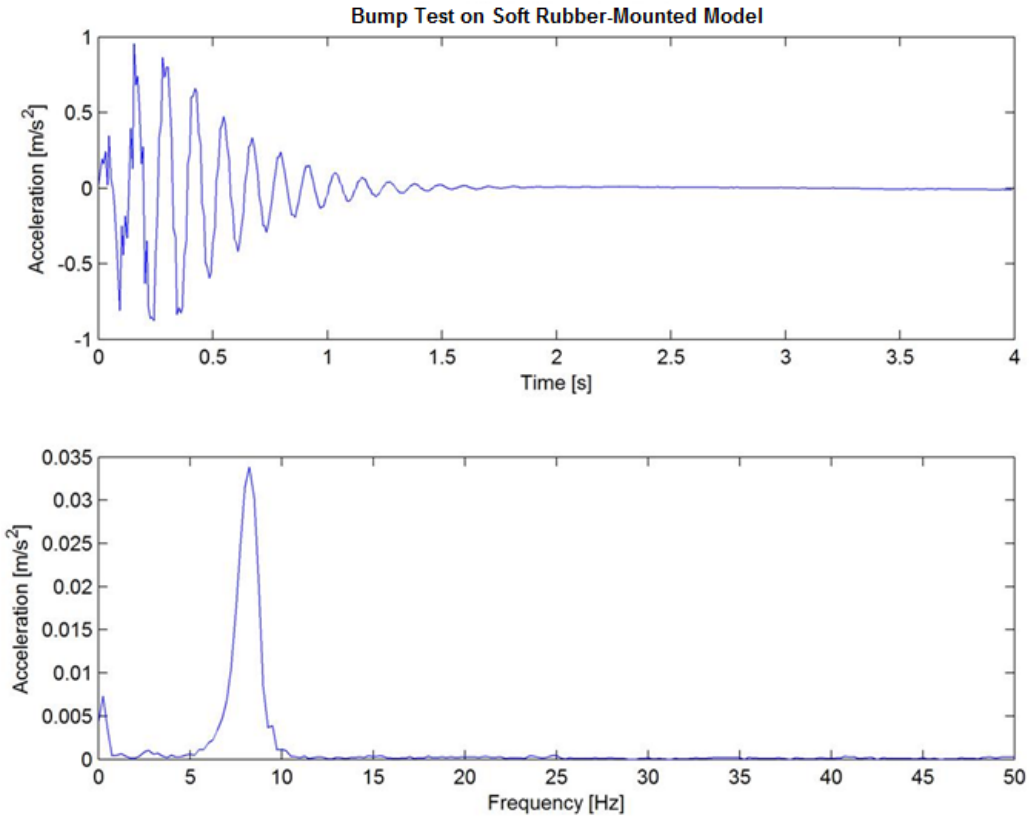

Figure 67: Measured results from the bump test on the soft rubber-mounted model

This bump test results showed the true complexity of the system in the real-world. Each of these amplitude peaks was characteristic of one natural frequency and could be described separately.

The first pronounced peak was the bounce natural frequency (8.5 Hz) expected of the system in the direction of the bump, with the whole isolated model vibrating as one mass. This frequency was therefore the natural bounce frequency of the heat exchanger model in the horizontal direction.

The other peaks, especially in the area around 15 – 20 Hz, were assumed to be rotational natural frequencies of the system that were ignored when the model is only modelled in one direction.

In the stiff steel-mounted case these natural frequencies were at very high values, but as a complication of the introduction of the mounting system, these natural frequencies were also lowered.

The second natural frequency that was expected higher than the 18.375 Hz measured in Figure 55, could only be identified by very small peaks due to the difficulty in exciting this mode shape.

The difficulty in exciting the mode shape during the bump test could be due to the mounts being much less stiff than the plates. This could have had the result that the energy that was intended to excite the second mode shape, would rather excite the less stiff mode shapes than the stiffer ones.

To ensure that the peaks that were observed between 23 Hz and 25 Hz was the second natural frequency that was sought, the model was subjected to a number of forcing frequencies between 20 Hz and 30 Hz, which clearly indicated that a natural frequency existed in the vicinity of about 24.5 Hz.

To ensure that the top and the bottom mass was moving out of phase with each other, as expected from the second natural frequency, the measurements were saved and evaluated, an extract of the measurements are shown in Figure 68.

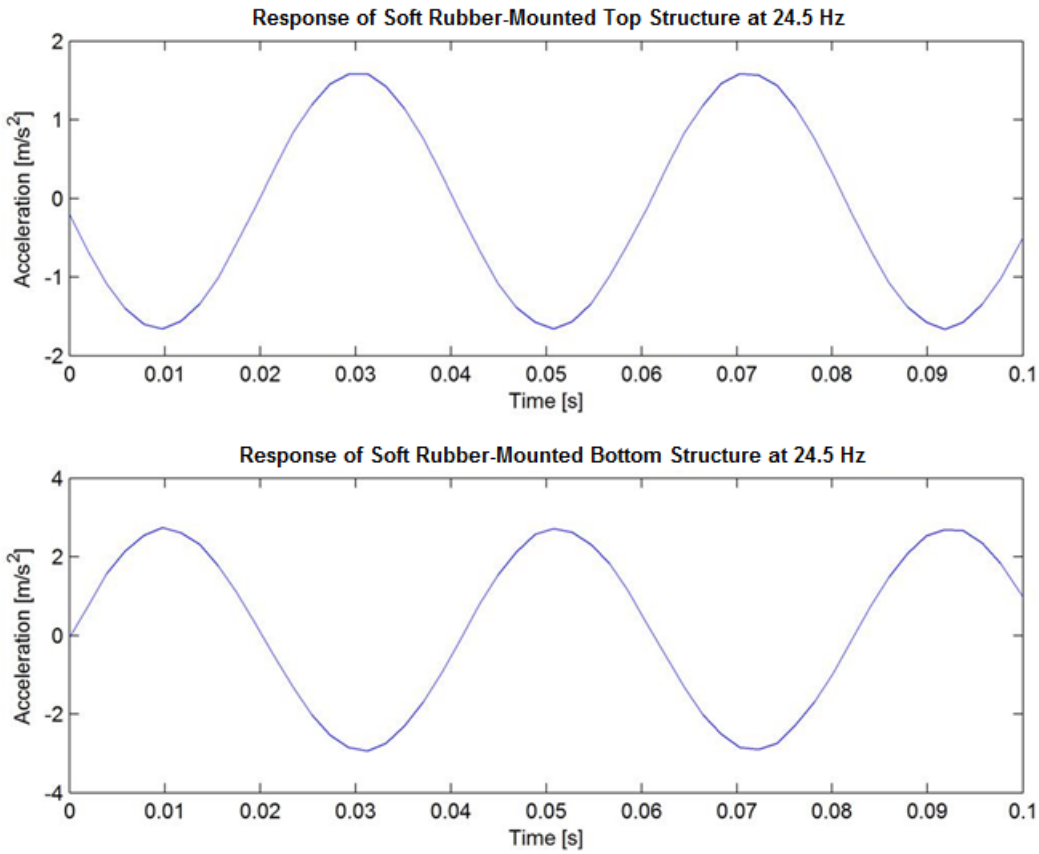

Figure 68: A comparison between the measured response of the two points at 24.5 Hz

This data clearly showed that the top and the bottom of the structure moved out of phase and confirmed the suspicion that this was indeed the second natural frequency of the soft rubber-mounted model.

From the measured natural frequencies in this section, together with the measured natural frequency of the model in the stiff steel-mounted case (section 7.2), the natural frequencies of the system can be summarised as shown in Table 10.

Table 10: Measured natural frequencies of the experimental model

	Stiff steel-mounted case	Soft rubber-mounted case
First natural frequency [Hz]	18.375	8.5
Second natural frequency [Hz]	-	24.5

7.6. Characterisation of amplitude of oscillating force

As stated in Section 6.1, a vibrating motor is used to simulate the fluid-induced force on the panels of the heat exchanger model. Due to the fact that the adjustment of the unbalanced force was not as accurate as required, the values were experimentally characterised over a number of frequencies.

The motor induced a vibration by rotating an unbalanced load around the axis at a speed measured in radians per second (ω). According to Stadelbauer, the force due to an unbalanced mass can be described by Equation (7.8)(Stadelbauer, 2002).

$$F = m_u r \cdot \omega^2 \tag{7.8}$$

The radial force on the shaft is therefore determined by the size of the unbalanced mass of the rotating shaft (m_u), the distance between the centre of gravity and the centre of rotation (r) and the velocity of the rotation (ω).

In the case of the vibrating motor, the mass of the shaft and the distance between the centre of gravity and the centre of mass were not known. The rotational speed, however, was easy to obtain from the frequency of the variable speed drive, or the frequency of the response.

As the actual individual values of the unbalanced mass (m_u) and the radial distance (r) are not essential for this case, the experiment was, therefore, designed only to determine the product of the two values ($m_u r$).

The vibrating motor was mounted on four metallic springs (to minimise the amount of damping), with an accelerometer in the vertical position as can be seen in Figure 69.

Figure 69: Experimental setup used to determine oscillating force

To determine the stiffness of the springs, a vertical bump test was performed. The frequency response of this test can be seen in Figure 70.

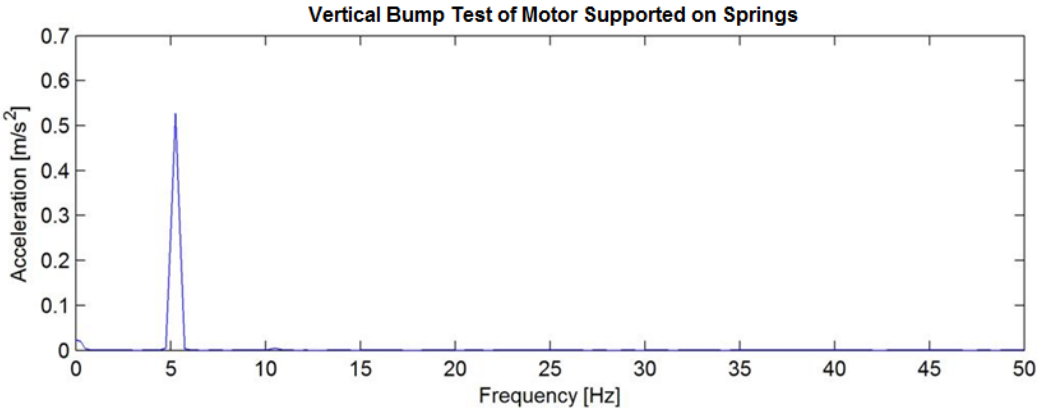

Figure 70: Measured frequency response of motor bump test

The results indicate the system natural frequency at 5.25 Hz (32.987 rad/s), with the mass of the motor, from Table 2, the stiffness of the springs can be determined. The calculation of the stiffness of the four springs is shown in Table 11.

Table 11: Calculation of stiffness of four springs

Mass [kg]	m_m	6.274
Natural frequency [rad/s]	ω_n	32.987
Stiffness of 4 Springs [N/m]	k	6827

The system is fully characterised if the mass of the motor and the stiffness of the springs were known. The unbalanced force could, therefore, be determined by measuring the response of the system under a stable forcing frequency.

From the displacement amplitude (X), the force (F_0) can be determined with the stiffness of the plate pack (k_p) taken into account, using Equation (7.9), which is derived from the equations of motion for a one DOF system (Rao, 2004).

$$F_0 = X \cdot \left(k - m_m \cdot \omega^2\right) \tag{7.9}$$

The vibration response was measured for four different forcing frequencies to ensure that the values obtained are accurate. With Equation (7.8), the unbalanced load factor ($m_u r$) for each case could be determined. The average unbalanced load factor was taken to represent the correct value over the whole range of operation. The calculation of the average unbalanced load function can be seen in Table 12.

Table 12: Calculation of the average unbalanced load factor

f [Hz]	**ω [rad/s]**	**$\ddot{X}$ [Gs]**	**$\ddot{X}$ [m/s2]**	**X [m]**	**$F0$ [N]**	**$m_u r$ [kg.m]**
15	94.248	0.370	3.630	-4.086E-04	19.983	0.00224968
19	119.381	0.557	5.464	-3.834E-04	31.665	0.00222182
23	144.513	0.803	7.877	-3.772E-04	46.848	0.00224324
29	182.212	1.255	12.312	-3.708E-04	74.711	0.00225024
					Average	0.002238244

With this value, the amplitude of the oscillating force can be determined for any forcing frequency by using Equation (7.10).

$$F_0 = 0.002238244 \cdot \omega^2 \tag{7.10}$$

As can be seen from the calculated values in Table 12, the calculated values for $m_u r$ over the entire range compared excellently with each other. This can be seen as confirmation that the unbalanced load was accurately characterised.

7.7. Conclusion

The mass, stiffness and damping characteristics of all the relevant components were experimentally verified individually. Table 13 gives a summary of all the element values together with the source of the value.

The components were then assembled into the final experimental configurations and subjected to bump tests and forced frequencies to ensure that the experiment as a whole reacted predictably and results obtained could be replicated time after time. The natural frequencies of the combined system were measured to facilitate the comparison with the theoretical predictions.

Table 13: Summary of characterized element values

Variable	Value	Unit	Source
m_1	22.255	kg	Table 7
m_2	24.007	kg	Table 7
k_{1R}	319996890	N/m	Equation (7.2)
k_{1M}	160837	N/m	Equation (7.4)
k_2	319997	N/m	Equation (7.1)
k_3	36529	N/m	Equation (7.5)
c_{1R}	0	N.s/m	Equation (5.28)
c_{1M}	300.280	N.s/m	Equation (7.6)
c_2	43.699	N.s/m	Equation (7.3)
c_3	26.830	N.s/m	Equation (7.7)

To eliminate the uncertainty of the exact amplitude of the exciting force, the force was measured over a range of forcing frequencies to determine an equation to accurately determine the force for any frequency.